A&A 485, 51–61 (2008)
DOI: 10.1051/0004-6361:200809806

Astronomy & Astrophysics

Long-term radio variability of AGN: flare characteristics

T. Hovatta[1], E. Nieppola[1], M. Tornikoski[1], E. Valtaoja[2,3], M. F. Aller[4], and H. D. Aller[4]

[1] Metsähovi Radio Observatory, TKK, Helsinki University of Technology, Metsähovintie 114, 02540 Kylmälä, Finland
e-mail: tho@kurp.hut.fi
[2] Tuorla Observatory, University of Turku, Väisäläntie 20, 21500 Piikkiö, Finland
[3] Department of Physics, University of Turku, 20100 Turku, Finland
[4] Department of Astronomy, University of Michigan, Ann Arbor, MI 48109, USA

Received 19 March 2008 / Accepted 18 April 2008

ABSTRACT

Aims. We have studied the flare characteristics of 55 AGN at 8 different frequency bands between 4.8 and 230 GHz. Our extensive database enables us to study the various observational properties of flares in these sources and compare our results with theoretical models.
Methods. We visually extracted 159 individual flares from the flux density curves and calculated different parameters, such as the peak flux density and duration, in all the frequency bands. The selection of flares is based on the 22 and 37 GHz data from Metsähovi Radio Observatory and 90 and 230 GHz data from the SEST telescope. Additional lower frequency 4.8, 8, and 14.5 GHz data are from the University of Michigan Radio Observatory. We also calculated variability indices and compared them with earlier studies.
Results. The observations seem to adhere well to the shock model, but there is still large scatter in the data. Especially the time delays between different frequency bands are difficult to study due to the incomplete sampling of the higher frequencies. The average duration of the flares is 2.5 years at 22 and 37 GHz, which shows that long-term monitoring is essential for understanding the typical behaviour in these sources. It also seems that the energy release in a flare is independent of the duration of the flare.

Key words. galaxies: active – radio continuum: galaxies

1. Introduction

Active galactic nuclei (AGNs) exhibit variability across the whole electromagnetic spectrum, and it is often possible to see distinct flares in their flux density curves. By studying the differences in the variability of the various AGN types we gain understanding into the physics involved in producing these events. The study of the radio regime is of special interest because it relates directly to the shock development in the jets.

Variability studies of a large sample of AGNs at lower radio frequencies of 4.8−14.5 GHz have been done at the University of Michigan Radio Observatory (UMRAO), where AGNs have been monitored since the 1960s. Hughes et al. (1992) studied the long-term variability time scales of quasars and BL Lacertae objects (BLOs). Aller et al. (1999) studied the total flux density and linear polarisation properties of BLOs and Aller et al. (2003) the variability of the complete Pearson-Readhead radio sample.

At Metsähovi Radio Observatory AGNs have been monitored at 22 and 37 GHz for almost 30 years. Variability studies were first performed after 5 years of observations (Valtaoja et al. 1988; Valtaoja et al. 1992a,b) and updated by Lainela (1994) with 12 years of data. Long-term variability time scales were studied by Lainela & Valtaoja (1993) and Hovatta et al. (2007). Southern AGNs were studied at the higher frequencies of 90 and 230 GHz by Tornikoski et al. (1993) and Tornikoski et al. (2000). Also Ciaramella et al. (2004) studied the variability properties of a sample of AGNs using the data from UMRAO and Metsähovi.

Apart from these studies, most of the work done on the variability of AGNs concentrates on individual sources and their multifrequency behaviour. For example, in Pyatunina et al. (2006) and Pyatunina et al. (2007) seven AGNs are studied at 4.8−37 GHz. They decompose the flux density curves into Gaussian flares and study the properties of the flares and also the duty cycles in these sources. While this can describe and model one source very well, studies of large samples are important so that statistical differences between the source types can be studied.

The flares in the radio regime are explained by adiabatic shock-in-jet models (Marscher & Gear 1985; Hughes et al. 1985). In these models an adiabatic shock is formed somewhere in the base of the jet and as it moves downward in the jet, we see synchrotron radiation at different frequencies and the observed properties depend on the phase of the shock development. According to the model by Marscher & Gear (1985) the shock goes through three phases: the growth stage where Compton losses dominate and the flux density increases at all frequencies, a plateau stage where the energy gains and losses are equal and the peak frequency moves to lower frequencies, and a decay phase where adiabatic losses start to dominate and the flux density declines.

Valtaoja et al. (1992a) developed a parametrisation of the Marscher & Gear model – a generalised shock model – where the observed properties depend on the peak frequency of the synchrotron flare and how it relates to the observing frequency. If the peak frequency $\nu_{\rm max}$, where $S(\nu_{\rm max})$ reaches its highest value, is higher than the observing frequency $\nu_{\rm obs}$, the flare is classified as a high-peaking flare. In this case the shock reaches its maximal development above the observing frequency and is in its decaying stage when observed. We should also see time delays towards lower frequencies. The flare is called low-peaking if $\nu_{\rm obs} > \nu_{\rm max}$. Now the shock is in its growing stage when observed and flux

density curves of nearby frequencies trail each other closely and there should not be any time delays.

This model can be tested by studying individual flares in AGNs. In this paper we used the Metsähovi monitoring sample as a starting point and extracted 159 individual flares from the flux density curves of 55 sources. We used 8 different frequency bands between 4.8 and 230 GHz to study the flare development. We also conducted a basic variability analysis by calculating the variability indices.

The paper is organised as follows: in Sect. 2 we describe the source sample and data used. The methods used are described in Sect. 3. Section 4 includes the results of our analysis and the discussion follows in Sect. 5. The conclusions are drawn in Sect. 6. We use the value $H_0 = 72$ km s^{-1} Mpc^{-1} throughout the paper. All the statistical analyses have been performed with the Unistat statistical package for Windows[1] (version 5.0).

2. Data and the sample

Our sample is selected from the Metsähovi monitoring sources (Salonen et al. 1987; Teräsranta et al. 1992, 1998, 2004, 2005) and from our monitoring sample of southern AGNs at the Swedish-ESO Submillimetre telescope (SEST) (Tornikoski et al. 1996). The criterium for selection was that there must be at least one well-sampled outburst at two of the frequency bands between 22 and 230 GHz. This criterium was fulfilled for 55 sources. The minimum relative flux density change in these outbursts was 0.5 Jy at 37 GHz and between 0.4 and 0.6 Jy at other frequency bands. In addition to the Metsähovi 22, 37 and 90 GHz and SEST 90 and 230 GHz data we used the lower frequency data at 4.8, 8 and 14.5 GHz from the UMRAO database. Higher frequency data at 90, 150 and 230 GHz were also collected from the literature (Steppe et al. 1988, 1992, 1993; Reuter et al. 1997). Some of the southern sources are not monitored at Metsähovi and thus have data only at the higher 90 and 230 GHz and the UMRAO low frequencies.

Many of the sources have been monitored for over 25 years and here we used data from the beginning of our monitoring in the 1980s until 2005. Our study also includes unpublished data at 37 GHz from December 2001 to April 2005 and at 90 and 230 GHz from the SEST from 1994.5−2003. The 37 GHz data for BL Lacertae objects from 2001−2005 are published in Nieppola et al. (2007). The observation method and data reduction process of Metsähovi data is described in Teräsranta et al. (1998).

Our sample consists of different types of AGNs, of which 14 sources are BLOs, 4 are radio galaxies (GALs), 20 are Highly Polarised Quasars (HPQs), 12 are Low Polarisation Quasars (LPQs) and for 5 sources we had no information about their optical polarisation and they are therefore considered to be LPQs in this study. The BLOs are studied in more detail in a separate paper (Nieppola et al. 2008). When studying the differences between the source classes GALs are not considered because of their smaller number in the study. The source sample is shown in Table 1, where the B1950-name, other name, classification, possible EGRET detection, number of flares, number of datapoints since 1980 in each frequency band, maximum observed flux density at 37 GHz, variability index at 37 GHz and the median duration of flares at 37 GHz are tabulated. There is a clear selection effect in the sample as only sources with distinct flares were selected for the analysis. The radio properties of these sources are interesting in view of the GLAST-satellite mission and therefore in Table 1 we have also marked the 29 sources that are high-confidence or possible detections of EGRET (Hartman et al. 1999; Mattox et al. 2001).

[1] http://www.unistat.com/

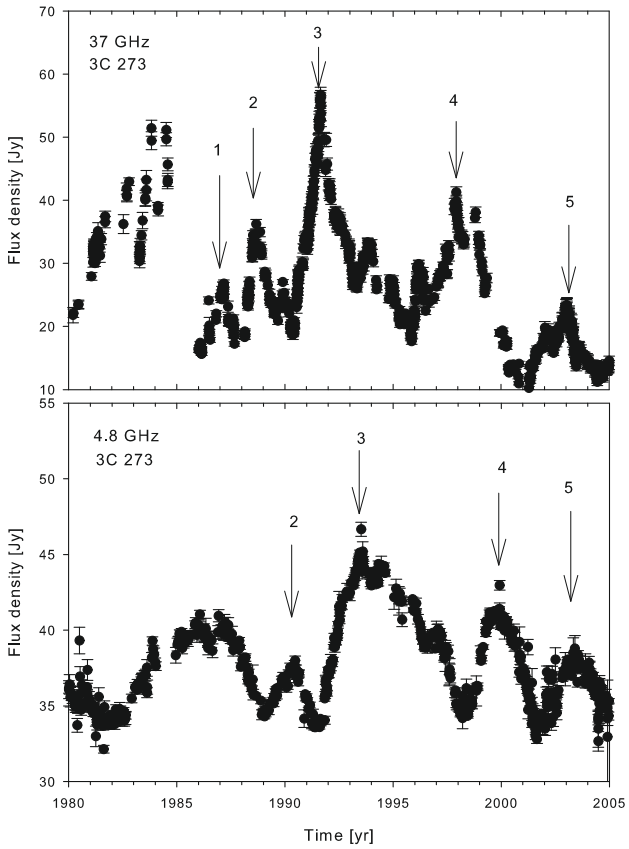

Fig. 1. *Upper panel*: flux density curve of the LPQ source 3C 273 (1226+026) at 37 GHz. Flares used in our analysis are marked with arrows. *Lower panel*: flux density curve at 4.8 GHz.

3. Methods

We separated each well-monitored flare within the flux density curves and determined their start, peak and end epochs and flux densities for those epochs. Figures 1 and 9 show examples of flux density curves. In Fig. 1 the analysed flares of the LPQ source 3C 273 (1226+023) are shown at 37 and 4.8 GHz. Altogether 159 flares fulfilled our criterium of being well-monitored in at least two frequency bands. From the start and end times we calculated the duration of the flares in the observer's frame, and using the peak epoch, also the rise and decay times at all frequency bands separately. In addition to the direct observational peak flux density of the flare, we used in our analysis the relative peak flux density, which is the peak flux density minus the start flux density. Our flares are distributed between the classes so that there are 46 flares in BLOs, 15 in GALs, 59 in HPQs and 39 in LPQs. This means that on average every BLO has 3.3 well-monitored flares during the 25 years while LPQs have one less (2.3). There are differences within the source classes as well. For example, the BLO source PKS 0735+178 has only one well-monitored flare during the 20 years' period it has been observed whereas BL Lac and OJ 287 both have 9 well-observed flares.

We note that our definition of individual flares is based on visual inspection and is clearly different compared to models where a theoretical flare form is fitted to the observations (e.g. Valtaoja et al. 1999; Türler et al. 1999). Here we have, however,

Table 1. The sample. For each source the number of flares, the number of datapoints since 1980 in each frequency band, the maximum flux density ($S_{\rm max}$), variability index V and median duration of flares at 37 GHz are listed. Column 4 indicates if the source is a high-confidence EGRET detection (x) or a possible detection (?).

B1950 name	Other name	Class	EGRET detection	Number of flares	Number of datapoints since 1980 in each frequency band								$S_{\rm max}$ [Jy]	V	Med duration [yr]
					4.8	8	14.5	22	37	90	150	230	37 GHz	37 GHz	37 GHz
0007+106	III ZW 2	GAL		6	234	438	477	309	253	26	–	15	3.08	0.84	1.82
0059+581		LPQ		2	–	–	–	148	101	–	–	–	5.23	0.70	2.47
0106+013	OC 012	HPQ		3	106	256	220	197	160	–	–	–	3.77	0.68	3.87
0109+224	S2 0109+22	BLO		3	114	152	162	181	152	–	–	–	3.13	0.78	3.01
0208−512		BLO	x	1	–	–	–	–	–	57	–	31	6.51[1]	0.66[1]	6.52[1]
0224+671		LPQ		2	110	115	114	106	80	42	–	–	3.06	0.65	1.99
0234+285	4C 28.07	HPQ	x	2	221	228	264	145	105	80	–	–	4.68	0.48	4.57
0235+164		BLO	x	4	723	1024	946	399	548	160	26	46	6.88	0.88	2.52
0333+321	NRAO 140	LPQ		2	–	–	–	178	153	–	–	–	2.68	0.56	5.49
0336−019	CTA 026	HPQ	x	2	178	506	433	108	82	67	–	–	3.86	0.51	2.45
0415+379	3C 111	GAL	?	3	232	471	425	147	88	29	–	–	10.22	0.65	2.13
0420−014	OA 129	HPQ	x	3	614	1042	917	378	417	198	–	59	15.68	0.76	3.48
0422+004	OF 038	BLO		2	165	516	373	144	131	44	–	20	2.40	0.76	1.96
0430+052	3C 120	GAL		4	621	1102	1003	417	462	109	–	–	5.45	0.54	2.05
0446+112	PKS 0446+112	GAL	?	2	–	–	–	119	70	–	–	–	2.76	0.73	3.46
0528+134	PKS 0528+134	LPQ	x	4	215	500	426	548	371	130	–	–	11.03	0.72	2.70
0537−441		HPQ	x	1	–	–	–	–	–	50	–	25	7.99[1]	0.64[1]	–
0607−157		LPQ		1	731	951	1002	–	–	75	–	27	9.65[1]	0.62[1]	1.75[1]
0642+449	OH 471	LPQ		1	–	–	–	270	219	47	–	–	3.94	0.44	3.59
0716+714		BLO	x	2	369	347	689	203	493	–	–	–	6.28	0.90	3.07
0735+178	PKS 0735+17	BLO	x	1	416	640	693	309	295	99	–	38	5.26	0.80	10.66
0736+017		HPQ		2	137	320	294	208	157	79	–	26	4.71	0.75	1.30
0754+100	OI 090.4	BLO		2	122	295	289	208	169	24	–	–	2.94	0.67	3.27
0804+499		HPQ	?	4	206	209	199	257	160	25	–	–	3.47	0.79	0.83
0827+243	OJ 248	LPQ	?	3	–	–	–	133	62	16	–	–	2.93	0.62	1.36
0847−120	J0850-1213	LPQ	x	3	–	–	–	331	131	–	–	–	3.66	0.69	1.54
0851+202	OJ 287	BLO	x	9	762	902	955	895	916	272	–	74	9.18	0.74	1.31
1055+018	OL 093	HPQ		4	354	573	639	255	229	80	–	27	7.05	0.60	2.61
1156+295	4C 29.45	HPQ	x	6	414	810	667	404	326	73	–	–	5.32	0.79	1.59
1222+216	PKS 1222+216	LPQ	x	2	–	–	–	243	116	27	–	14	2.65	0.74	2.38
1226+023	3C 273	LPQ	x	5	720	1033	951	939	1041	352	28	166	56.72	0.68	3.17
1253−055	3C 279	HPQ	x	6	774	1065	1039	762	790	234	28	122	34.48	0.66	2.50
1308+326	AU CV n	BLO		2	609	948	779	378	315	–	–	–	4.16	0.77	13.17
1334−127		HPQ	x	1	482	821	649	–	–	116	–	35	9.35[1]	0.60[1]	2.41[1]
1413+135		BLO		2	279	701	562	243	186	71	–	–	4.55	0.85	4.77
1502+106	OR 103	HPQ		3	–	–	–	156	136	–	–	–	2.28	0.57	1.98
1510−089	PKS 1510-089	HPQ	x	6	587	984	1081	245	263	111	–	39	5.83	0.74	1.50
1606+106	4C 10.45	LPQ	x	2	–	–	–	150	108	–	–	–	3.73	0.70	4.12
1611+343	DA 406	LPQ	x	1	–	–	250	229	198	–	–	–	5.23	0.54	4.60

Table 1. continued.

B1950 name	Other name	Class	EGRET detection	Number of flares	Number of datapoints since 1980 in each frequency band								S_{max} [Jy] 37 GHz	V 37 GHz	Med duration [yr] 37 GHz
					4.8	8	14.5	22	37	90	150	230			
1633+382	4C 38.41	LPQ	x	2	–	–	453	457	466	–	–	–	7.69	0.71	3.05
1641+399	3C 345	HPQ		3	987	1104	1018	806	783	182	40	–	17.03	0.64	4.46
1730−130	NRAO 530	LPQ	x	2	340	615	501	83	80	93	–	–	15.55	0.71	4.06
1739+522	S4 1739+52	HPQ	x	2	259	363	395	149	121	–	–	–	3.12	0.77	4.24
1741−038	PKS 1741-038	HPQ		2	–	222	299	272	296	111	–	–	8.93	0.70	3.03
1749+096	PKS 1749+096	BLO		5	695	1032	1088	583	465	154	–	51	10.09	0.85	0.94
1921−293		HPQ		1	401	694	657	–	–	120	–	45	15.47[1]	0.69[1]	10.68[1]
2007+776	S5 2007+77	BLO		1	232	–	436	92	84	–	–	–	2.97	0.67	3.34
2145+067		LPQ		4	304	821	818	551	496	134	–	34	11.77	0.41	3.12
2200+420	BL Lac	BLO	x	9	938	1115	1298	965	998	145	–	–	13.75	0.83	1.44
2201+315	4C 31.63	LPQ		2	–	–	–	280	251	–	–	–	6.38	0.62	4.55
2223−052	3C 446	BLO		3	532	770	837	237	240	145	–	39	10.86	0.63	5.84
2227−088		HPQ		1	–	–	–	33	27	20	–	14	3.03	0.74	3.56
2230+114	CTA 102	HPQ	x	1	–	983	909	295	293	106	–	–	7.57	0.62	2.23
2251+158	3C 454.3	HPQ	x	6	674	1070	1067	760	722	244	–	73	16.82	0.58	1.51
2255−282		LPQ		1	–	–	–	–	–	55	–	22	10.14[1]	0.76[1]	5.77[1]

[1] = Values taken at 90 GHz.

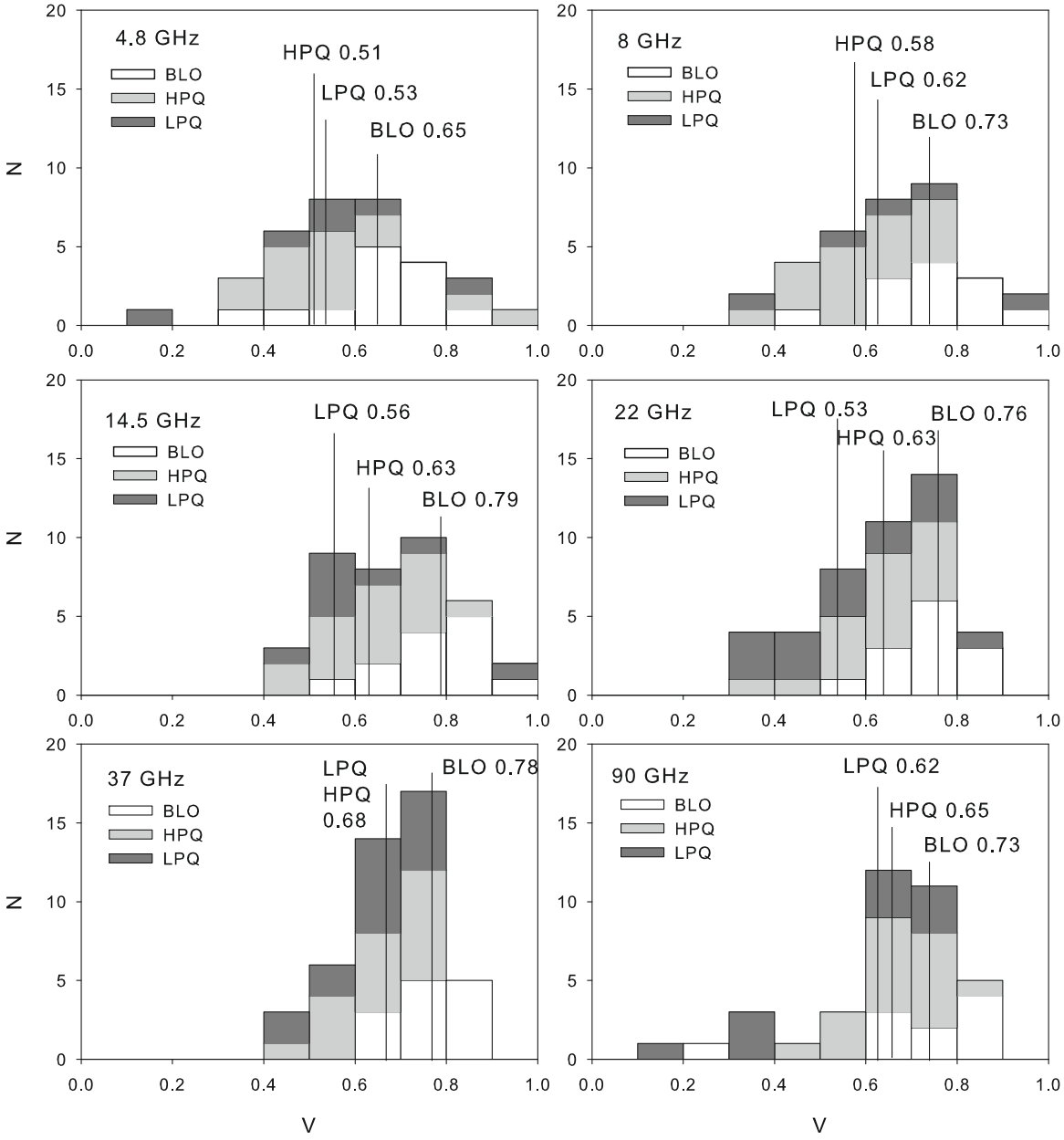

Fig. 2. Distribution of variability indices in different source classes and frequency bands. Median values for each source class are shown by vertical lines.

studied the observational properties of the flares and how they depend on each other. Therefore, a flare, as defined in this work, may include several individual shocks or events.

4. Variability properties

4.1. Variability indices

We calculated the variability indices V for each source at all the frequency bands as defined in Eq. (1)

$$V = \frac{(S_{\max} - \sigma_{S_{\max}}) - (S_{\min} + \sigma_{S_{\min}})}{(S_{\max} - \sigma_{S_{\max}}) + (S_{\min} + \sigma_{S_{\min}})}, \quad (1)$$

where $S_{\max}$ is the maximum observed flux density of the source and $\sigma_{S_{\max}}$ is its error and $S_{\min}$ and $\sigma_{S_{\min}}$ are the minimum flux density and its error. The distribution of the indices in the different source classes and at frequencies between 4.8 and 90 GHz are shown in Fig. 2, where also the median values are marked for each source class by vertical lines.

We ran the Kruskal-Wallis analysis (KW-analysis) to see if there are any statistically significant differences in the variability indices of the frequency bands and source classes. The only difference between the frequency bands was that the 4.8 GHz indices differ from most other frequencies significantly within the 95% confidence limit. The indices at 4.8 GHz are smaller than those at higher frequencies. This can be understood as towards the lower frequency bands the flares are observed later due to synchrotron self-absorption. The flux densities are lower, timescales are longer, and it is also more difficult to distinguish the individual subsequent flares from each other. This is clearly seen in Fig. 1 if the 4.8 GHz flux density curve is compared to the 37 GHz curve. The relative flux densities are much lower and many individual flares seen in the 37 GHz curve, for example the flare in 1996, cannot be separated in the 4.8 GHz curve.

Table 2. Median values of duration, observed peak flux density and relative peak flux density for all frequencies and source classes. Number of flares used to calculate the value is also shown.

ν [GHz]	Median duration [yr]									
	All	N	BLO	N	GAL	N	HPQ	N	LPQ	N
4.8	2.9	81	2.7	34	2.8	7	3.0	30	3.6	10
8	2.8	94	2.7	37	2.6	8	2.8	37	3.3	12
14.5	2.5	110	2.4	44	2.2	8	2.5	40	3.1	18
22	2.5	145	2.3	43	2.4	14	2.5	53	2.6	35
37	2.4	150	2.4	43	2.1	15	2.4	56	2.7	36
90	2.3	68	2.5	18	2.1	3	2.1	31	3.0	16
230	2.5	31	2.3	9	–	–	2.8	15	2.5	7
ν [GHz]	Median observed peak flux density [Jy]									
	All	N	BLO	N	GAL	N	HPQ	N	LPQ	N
4.8	4.0	85	3.2	34	5.0	8	3.7	33	8.1	10
8	4.6	99	4.3	38	3.9	8	4.5	41	10.2	12
14.5	5.0	117	4.2	45	3.6	9	5.1	44	10.0	19
22	4.4	153	4.9	45	3.1	15	4.9	56	4.3	37
37	4.6	153	5.1	45	3.1	15	4.6	56	4.4	37
90	4.9	72	4.6	18	3.7	4	5.0	34	8.1	16
230	5.1	33	3.4	9	1.2	1	5.2	16	7.0	7
ν [GHz]	Median relative peak flux density [Jy]									
	All	N	BLO	N	GAL	N	HPQ	N	LPQ	N
4.8	1.8	85	1.7	34	1.1	8	1.8	33	3.8	10
8	2.4	99	2.1	38	1.3	8	2.2	41	5.3	12
14.5	2.7	117	2.4	45	1.6	9	3.1	44	4.6	19
22	2.6	151	2.8	44	1.8	15	2.8	56	2.5	36
37	2.8	151	3.1	44	2.0	15	2.8	56	2.5	36
90	3.1	72	2.8	18	2.4	4	3.6	34	4.8	16
230	3.6	31	1.9	9	–	–	3.6	15	6.2	7

When studying the distributions it seems that the BLOs have larger variability indices than the quasars. This is also confirmed by the KW-analysis which gives statistically significant differences between BLOs and both quasar types at 14.5−37 GHz. At 4.8 and 8 GHz LPQs and BLOs do not differ significantly but this is probably due to the low number of LPQs at these frequency bands. At 4.8 GHz there are only 6 LPQs and at 8 GHz only 5. These are also the more extreme LPQs with higher variability. In general, the individual flares of relatively faint LPQs are often superposed at lower frequencies.

4.2. Flare amplitudes

The number of flares for which it was possible to determine the peak flux densities vary between the frequency bands. Most of the flares are defined at 22 and 37 GHz which were used for selecting the flares. We determined the observed peak flux density for 153 flares at 22 and 37 GHz whereas this was possible for only 33 flares at 230 GHz. The number of sources for which we were able to define the relative flux density is even smaller because it was not always possible to determine when the flare started and what was the flux density then, even if the observed peak flux density is defined. In some cases we used the next minimum after the flare for the relative flux density.

The observed peak flux densities and relative flux densities varied also significantly between the flares. The minimum peak flux density observed was 0.7 Jy and the maximum 56.9 Jy. Clearly there are always some extreme objects which make the scatter large but the median values of these parameters seem to describe the overall behaviour in each source class and frequency band quite well. The median values of observed peak and relative flux densities of the flares are shown in Table 2 for each frequency band and source class.

Considering the observed peak flux densities, there are no clear differences between the frequency bands according to the KW-analysis. When the relative peak flux densities are considered the KW-analysis shows that only the 4.8 GHz differs from the other frequency bands. Also the higher frequency bands from 14.5 GHz to 230 GHz form one group while the 8−22 GHz frequency bands form another group. The median values have an increasing trend in the relative peak flux densities as the frequency increases. It also appears that in BLOs and HPQs the flux densities are somewhat higher at higher frequencies but the difference is not large. For LPQs, the peak flux densities at the lower 4.8−14.5 GHz frequencies clearly differ from those at the higher frequency bands but this is probably due to the much smaller number of sources at these frequencies. As was already noted in the previous section, at lower frequencies the flares are more superposed and it is the extreme objects that stand out. The fainter sources do not show distinguishable flares at lower frequencies and therefore are not included in the calculations. This is also seen in the KW-analysis which shows that at 4.8 and 8 GHz the LPQs differ from the other classes significantly. At 14.5 GHz the difference with the higher frequencies is not as clear when the relative peak flux densities are considered. At the higher frequencies there are no significant differences between the source classes.

4.3. Flare intensity and duration

In some cases we could not calculate the duration of the flare because either the starting or ending point was not determined. This varied between the frequency bands so that we were able to calculate the duration for 150 flares at 37 GHz and for 31 flares at 230 GHz. The durations of the flares varied from 0.3 years to 13.2 years.

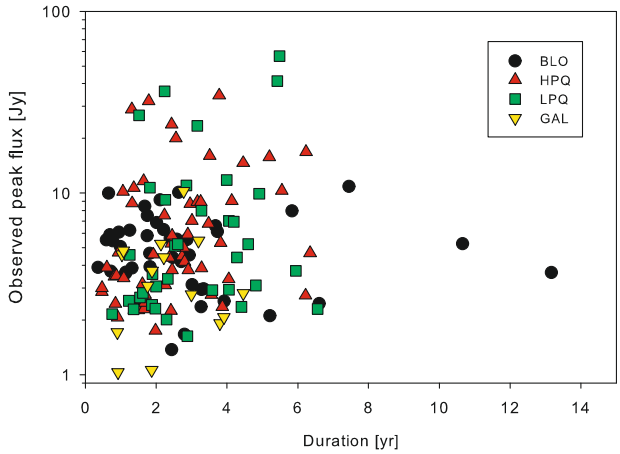

Fig. 3. Observed peak flux density against the duration of the flare at 37 GHz.

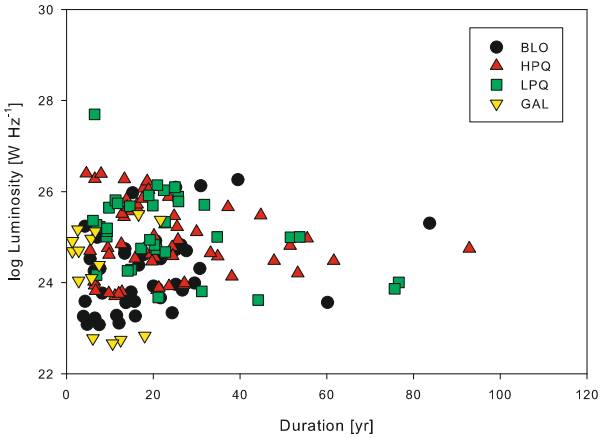

Fig. 4. Corrected peak luminosity at 37 GHz against the duration of the flare corrected for redshift and Doppler boosting.

The duration seems to decrease with increasing frequency but again the difference is not very large, only 0.6 years at most between 4.8 and 90 GHz. According to the KW-analysis there are also no significant differences between the source classes even though the LPQs seem to have slightly longer durations. This could indicate that there are differences in the physical conditions of the jets in LPQs and other classes. Of particular note is the long median duration of the flares: They last about 2.5 years at 22 and 37 GHz. This means that short multi-wavelength campaigns are not able to reveal the complete behaviour of these sources at radio frequencies. Long-term monitoring is needed to study the variability at these frequencies.

The rise and decay times appear to be approximately equal and so the flares are relatively symmetric. At 22 and 37 GHz the median rise times are 1 year and decay times 1.3 years in accordance with the results of Valtaoja et al. (1999). There are no significant differences between the frequency bands but the decay times of the LPQs seem to be slightly longer which is also seen in the KW-analysis.

In Fig. 3 we plotted the observed peak flux density of the flares against the duration for all sources at 37 GHz. The Spearman rank correlation for these parameters is $r = 0.15$ with probability $p = 0.03$. Thus the correlation is not strong. At lower frequencies the correlation was slightly higher, decreasing towards higher frequencies. If only quasars (HPQs and LPQs) are considered, there is a correlation of $r = 0.29$ with $p = 0.002$ at 37 GHz. The result is similar if HPQs and LPQs are treated separately. For BLOs there are no significant correlations (Nieppola et al. 2008).

There is a slightly higher positive correlation if the relative peak flux density is studied against the duration but the distribution of points looks very similar. At 37 GHz $r = 0.26$ with $p = 0.001$. Again the correlations at lower frequencies are slightly higher, decreasing towards higher frequencies. This time the correlation of quasars is even higher with $r = 0.36$ and $p = 0.0002$. Also in this case there are no correlations between these parameters if only BLOs are considered (Nieppola et al. 2008).

There is a selection effect which could affect the results. There are fewer weak flares of long duration. If such a flare is seen on the flux density curve, it may get overlooked as it resembles more a secular baseline flux density trend than a flare. Also the shorter the flares are, the more they show up like spikes in the flux density curve and are taken as flares more easily.

One other significant effect is Doppler boosting. When the sources are more boosted, their flux density levels are higher and at the same time the flares appear shorter. Therefore we corrected the peak flux density and duration for redshift and Doppler boosting using Eqs. (2) and (3) (e.g. Kembhavi & Narlikar 1999)

$$t_i = t_0 \frac{D_{\rm var}}{1+z} \tag{2}$$

$$L_i = S_0 \frac{4\pi D_{\rm L}}{1+z} \left(\frac{1+z}{D_{\rm var}} \right)^3 , \tag{3}$$

where t is the duration, S_0 is the flux density, $D_{\rm L}$ is the luminosity distance, z is the redshift and $D_{\rm var}$ is the Doppler boosting factor taken from Hovatta et al. (in preparation) where also other jet parameters such as jet speed are studied in more detail. When the corrected durations are studied there are still no clear differences between the frequency bands according to the KW-analysis. The LPQs have slightly longer flares but the difference is smaller than in the uncorrected case. Instead, at the lower 4.8−14.5 GHz frequencies the BLOs differ from the other source classes due to their shorter flares. The corrected peak luminosity against the corrected duration is shown in Fig. 4. The positive correlation disappears and there are no significant correlations according to the Spearman rank correlation.

4.4. Correspondence to the generalised shock model

According to the generalised shock model (Valtaoja et al. 1992a), the observed properties of a flare depend on the observing frequency and whether the peak frequency of the flare is higher or lower than the observing frequency. We studied how well these 159 flares correspond to the model by calculating a few parameters for each flare. We point out, however, that in this work we have not extracted separate shock events from flares but treated each longer outburst event as an individual flare.

First we determined the frequency band in which the flare occurs first and we have given it rank number 1. The second frequency band then gets number 2 and so on. For example, if the flare peak is first at 90 GHz, then at 22 GHz and then at 37 GHz, the rank numbers are 1 for 90 GHz, 2 for 22 GHz and 3 for 37 GHz. In this procedure we ignored flares which are clearly multi-peaked and for which it is impossible to determine the actual peak at all frequency bands. We have not ignored frequencies with larger gaps and therefore we expect scatter in

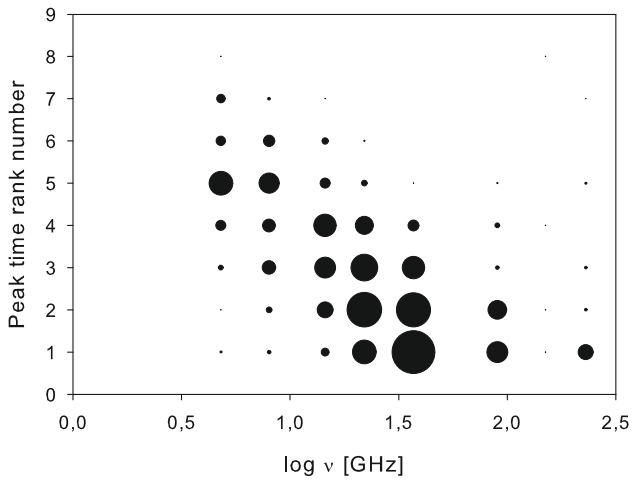

Fig. 5. Peak time rank number plotted against the frequency. The frequency band having the flare peak first has been ranked 1.

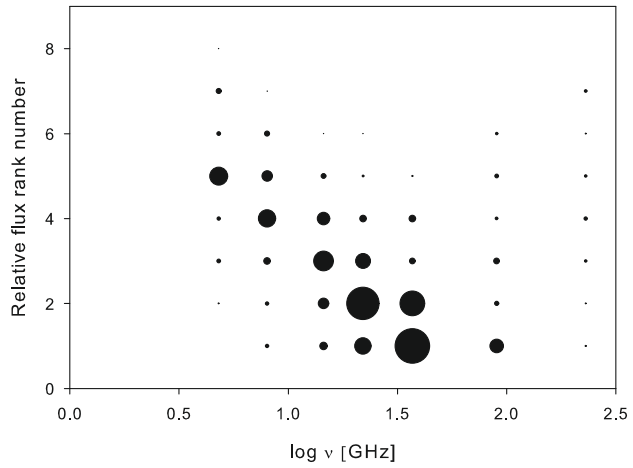

Fig. 6. Relative flux density rank number plotted against the frequency. Frequency with highest relative flux density has been ranked 1.

the results. We plotted the peak time rank numbers against the frequency in Fig. 5 in a bubble plot. The bigger the bubble, the more cases there are in that rank number and frequency. The plot shows that, as expected, the flares are peaking first at higher frequencies but there are also outliers and scatter.

Another prediction of the model is that relative flux density should be highest at the peak frequency, which in the case of high-peaking flares should be in the upper part of our frequency range. We made a similar bubble plot of the relative flux density rank number against the frequency (Fig. 6). In this case we have given rank number 1 to the frequency at which the relative flux density is highest. Rank number 2 is given to the frequency which has the second highest relative flux density and so on. Figure 6 shows that the highest flux density is usually at 22 and 37 GHz, although the number of flares at higher frequencies is lower and therefore the result could be slightly biased. Also the sampling of the higher frequencies is more sparse and therefore the actual flare peaks could have been missed in the observations.

A more straightforward way of studying the correspondence between the model and the observations is to normalise the relative flux density to the flux density of the peak frequency $\nu_{\rm max}$ of the flare. In our analysis we have simply taken $\nu_{\rm max}$ as the frequency band at which the relative peak flux density is highest. A

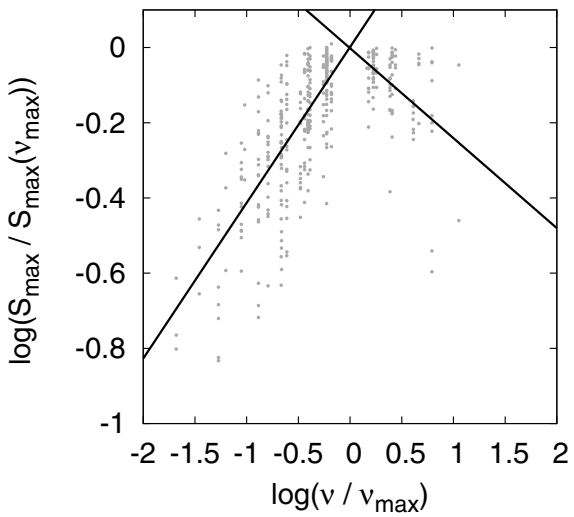

Fig. 7. Observed maximum relative flux density scaled to the frequency at which the maximum occurs. The two straight lines give best fits to the section below and above the peak frequency.

more accurate way would be to interpolate the peak frequency but we find it unsuitable for our data which has large gaps especially at the higher 90 and 230 GHz frequency bands, making the estimation of the true peak time and peak flux density of the flare difficult. According to Valtaoja et al. (1992a) the maximum flux density of the flare should correspond to the plateau stage in the generalised model. Frequencies higher than $\nu_{\rm max}$ correspond to the growth stage and should have $\Delta S_{\rm max} \propto \nu^{\alpha_{\rm thin}}$. Frequencies lower than $\nu_{\rm max}$ should have $\Delta S_{\rm max} \propto \nu^{\rm b}$, where b depends on the model. This approach was originally used by Valtaoja et al. (1992a) and later by Lainela (1994). They used a smaller sample of sources and as the sources had been monitored for only a short time, they used the overall minimum and maximum values ever observed as the relative flux density. Our approach should be more accurate as the flares were individually separated and the number of flares is much higher.

In Fig. 7 we plotted the normalised relative flux density against the normalised frequency. All the values were normalised to the frequency at which the relative flux density is the highest. We also fitted straight lines to below and above the peak frequency. We can see that there is large scatter in the values but the trend is very much as expected when compared to the model in Valtaoja et al. (1992a). The fit gives $\Delta S_{\rm max} \propto \nu^{0.41}$ for the rising part and $\Delta S_{\rm max} \propto \nu^{-0.24}$ for the declining part. We also fitted the data separately for quasars and HPQs and LPQs and the results were very similar to those of the whole sample. According to the model, there should be a plateau between the slopes which is not seen in our analysis. We also tried to fit a plateau stage into the model, but two linear components describe the data more accurately. The same result was already obtained in Valtaoja et al. (1992a). They got a slope of 0.52 for the rising part and −0.26 for the declining part, which are very close to the values obtained here. Stevens et al. (1994) also obtained a value of −0.28 for the declining part in their study of 17 blazars between 22 and 375 GHz.

Time delays between the frequencies are also important but more difficult to study. This is because the sampling is often sparse and the actual peak time could have been missed during observations. If a source is observed once in two weeks, which is quite a common sampling rate for these sources at Metsähovi, the peak can occur at any time within a month. Often the gaps are

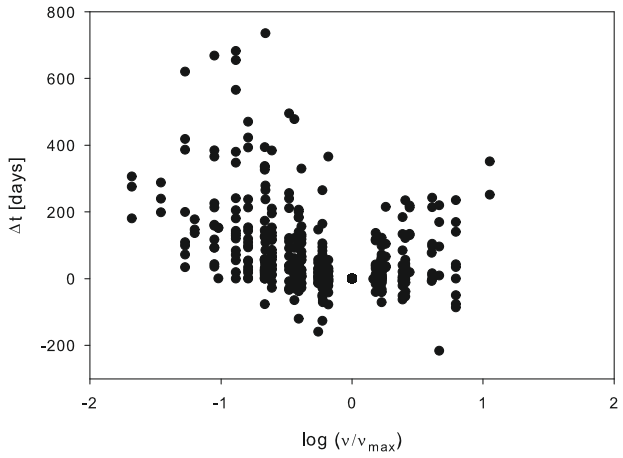

Fig. 8. Time delay between the observing frequency and peak frequency against the normalised frequency.

longer due to weather constrains or maintenance. Therefore any time delays shorter than a month are not reliable. At the higher 90 and 230 GHz frequencies the situation is even worse because the flares are faster and the data acquisition is even more sparse.

We calculated median time delays at different frequency bands and for 37 GHz it is 34 days, increasing towards lower frequencies and being 181 days at 4.8 GHz. According to the generalised shock model, there should not be significant time delays above the peak frequency but below it they should increase. We calculated the time delays between the peak frequency and other frequencies and plotted them against the normalised frequency in Fig. 8. It is clear that the trend is correct with time delays being larger at frequencies lower than the peak frequency. There is also large scatter in the values which is expected because the time delays are so difficult to determine especially at higher frequencies. In this analysis we took into account all flares where the peak was not clearly different at different frequencies and we did not ignore flares with poor sampling. Even time delays as large as 300 days can be due to poor sampling at 230 GHz. However, if compared to the model in Valtaoja et al. (1992a), we see clear correspondence between the model and observations.

We also studied one individual source, 0235+164, and its flare in 1993 in more detail. Figure 9a, shows the flux density curve of the source at 37 GHz, with every flare analysed for this source marked using arrows. Figure 9b shows the 1993 flare in more detail at 37 GHz. We have marked seven epochs of the flare and constructed simultaneous spectra at every epoch at all the frequencies used in the analysis (Fig. 9c). The spectra are simultaneous within two weeks but the 230 GHz points are in general more uncertain because of the more sparse sampling. The flare follows the shock model quite well with the flux density first rising at all frequencies. When the flux density starts to decay the peak of the spectrum moves to lower frequencies. No clear plateau is seen in this flare which agrees with the general results for the whole sample.

5. Discussion

We have studied the observational properties of radio flares for a large sample of densely monitored variable AGNs. For many of the sources the data sets span more than 25 years. For this study we only chose objects with clearly distinguishable radio flares, which biases this sample towards sources with notable variability and flares with relatively simple morphology.

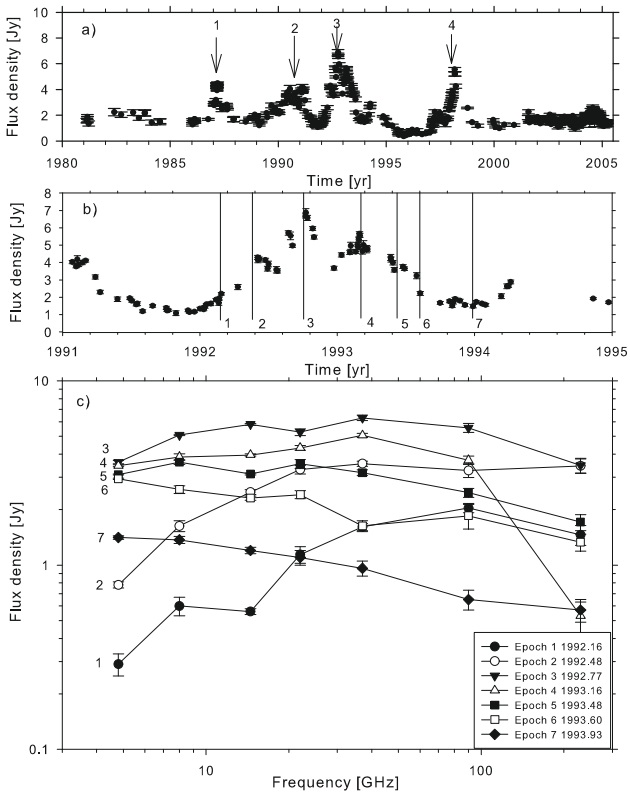

Fig. 9. a) Flux density curve of the BLO source 0235+164 at 37 GHz with each flare analysed marked with arrows. **b)** Flare number 3 in more detail. **c)** Spectra of every epoch marked in **b)**.

Within our sample, the BLOs have higher variability indices than quasars. This is in part caused by the fact that only the BLOs with truly distinct variability features were included in this study. Compared to the variability indices obtained in Nieppola et al. (2007), our indices are higher, the median variability indices of BLOs being 0.78 in this study and 0.33 in Nieppola et al. (2007).

The sample of Nieppola et al. (2007) also includes fainter BLOs for which no well-structured radio flares could be extracted from the flux density curves. The differences between the variability behaviour of these two BLO samples can be explained by the fact that only a small minority of the full BLO sample actually shows any extreme behaviour in the radio domain, most of them being faint and relatively non-variable even over several years of monitoring observations. However, it is noteworthy that the large BLO sample of Nieppola et al. (2007) only includes 5 years of data compared to our 25 years, and at least some of the sources may radically change their behaviour over longer timescales, as discussed in Hovatta et al. (2007).

Earlier studies of higher 90 and 230 GHz variability indices were done by Tornikoski et al. (1993) and Tornikoski et al. (2000). Their sample included southern AGNs observed with the SEST telescope. The variability indices are significantly lower than what we have obtained (for comparison we calculated the variability index defined as $(S_{\max} - S_{\min})/S_{\min}$ for our sample) but also the number of datapoints is much smaller. The average number of datapoints in our sample is almost five times larger. In Tornikoski et al. (2000) the effect of the number of datapoints was studied and they noticed that the variability indices increased with increasing number of datapoints, confirming our findings where only very long-term monitoring reveals the true

minimum and maximum flux densities of most sources. Even though the highest flux densities during flares are typically observed in the 37 and 22 GHz frequency bands (as seen in Fig. 6), the 90 GHz variability indices obtained in this paper are of the same order as those in the lower frequency bands, indicating that strong flares can indeed occur also in the mm-domain.

When we studied the duration and intensity of the individual flares, it was evident that most flares are very long lasting. The median duration of flares at 22 and 37 GHz is 2.5 years, which means that short-term observing campaigns are rarely helpful for describing the "typical behaviour" of these sources. When we add to this the result from Hovatta et al. (2007) that for these sources flares occur on average every 4−6 years, we can conclude that monitoring campaigns lasting at least ca. 5−7 years are needed in order to catch a typical source both in a quiescent and flaring state and to follow the flare evolution from the beginning to the end.

The flare intensities increase with flare duration only to some degree. For flares lasting 2−3 years we can see almost as high peak flux densities (observed peak flux density as well as the relative flux density during the flare) as for those lasting a few years longer. A striking result is that when we calculate the Doppler-corrected peak luminosities of these flares, the weak positive correlation disappears altogether and there is no correlation between the Doppler corrected peak luminosity against the Doppler corrected flare duration. This means that the energy release in a flare does not increase with duration for these flares.

When studying the rise and fall times of the flares we see that flares in general have semi-symmetric shapes, with the decay time typically being 1.3 times the rise time. The morphologies of flares are typically not very simple, though, and flares with multiple peaks or other finer structure complicate the analysis. In general, flares at 37 GHz or lower frequencies rarely consist of smooth rise and decay components only, and a more thorough analysis is needed to fully understand the physical characteristics of radio flares and to separate the individual flare components (Hovatta et al., in preparation).

Based on the observational results of this study, we have studied the correspondence between the observations and the generalised shock model by Valtaoja et al. (1992a). For 99 flares we had an estimate of the time delays between at least 3 frequency bands. Nearly half of them (46 flares) seemed to behave as the shock model predicts with no time delays above the peak frequency and increasing time delays below it. In addition in 34 cases the time delays were shorter than the sampling rate and therefore we cannot say whether they follow the shock model or not. Only in 20% (19 cases) the time delays and amplitudes did not follow the shock model. In these cases, however, the flares were defined to have multiple peaks and therefore the time delays were difficult to determine. Also the sampling rate may have been poor. In any case the flares seem to follow the shock model in general, even though there is large scatter due to poor sampling and complicated structure of the flares at different frequency bands. Of the well-determined flares where we could study if they are high- or low-peaking, 25 were high-peaking and 3 low-peaking at 22 and 37 GHz. This indicates that the peak frequency of the flares in these sources is somewhere in the millimetre domain. This is in agreement with Stevens et al. (1994) who found that in their sample of 17 blazars studied at 22−375 GHz the peak was at 90 GHz or below. Our results for the whole sample are very similar to those for BLOs studied in Nieppola et al. (2008).

When we studied the shape of the flare spectra normalised to the peak frequency, we found the best fit to be $\Delta S_{\rm max} \propto \nu^{0.41}$ for the rising part and $\Delta S_{\rm max} \propto \nu^{-0.24}$ for the declining part. We did not find a plateau between the slopes which is contradictory to the model but in agreement with earlier studies by Valtaoja et al. (1992a) and Lindfors et al. (2006). The declining slope $\alpha = -0.24$ corresponds to the optically thin spectral index $\alpha_{\rm thin}$ for a power-law electron energy distribution $N(E) \propto N_0 E^{-s}$ with $s = 1.5$ (Valtaoja et al. 1992a). This is slightly flatter than what is obtained for 3C 273 in Türler et al. (2000) and for 3C 279 in Lindfors et al. (2006), where values close to $s = 2$ were obtained. In their studies the flare spectra were flattening from $\alpha_{\rm thin} = -1.1$ to $\alpha_{\rm thin} = -0.5$ as the flare evolved. This is in accordance with the original shock model by Marscher & Gear (1985). In Stevens et al. (1994) the declining slope of −0.28 was explained as being due to the radiation being only partially thin close to the turnover frequency. This would cause the points to deviate from a straight line in the declining part of the spectrum. Also, data at sub-mm frequencies above 230 GHz would be required to estimate the accurate value of $\alpha_{\rm thin}$. The rising slope of 0.41 is in agreement with the original shock model (Marscher & Gear 1985) and also independently obtained in Valtaoja et al. (1992a). Therefore we consider our results to be in good agreement with the models, considering the scatter in our data.

6. Conclusions

In this paper we studied the long-term radio variability of a sample of 55 AGNs. We divided the flux density curves into individual flares and studied the properties of 159 well-monitored flares in at least two frequency bands between 4.8 and 230 GHz. Our main results can be summarised as follows:

1. The flares last on average 2.5 years at 22 and 37 GHz and are only slightly longer at lower frequencies. This has important consequences when planning multifrequency campaigns, which usually last only from a couple of days to months and therefore are unable to capture a radio flare as a whole.
2. There are no significant differences between the different source classes when the durations of the flares are studied although there is weak evidence for longer flares in the LPQs. When Doppler-corrected durations are studied the LPQs still have the longest flares but the difference is smaller. Also, the BLOs with their shorter flares differ from other source classes at the lower 4.8−14.5 GHz frequencies.
3. When studying the duration of the flares against the intrinsic Doppler-corrected peak luminosity, we found no correlation indicating that the energy release in a flare does not increase with duration for these flares.
4. The flares seem to follow the generalised shock model by Valtaoja et al. (1992a) quite well even though there is large scatter due to incomplete sampling and complicated structure of the flares at different frequency bands.

Acknowledgements. We acknowledge the support of the Academy of Finland (project numbers 212656 and 210338). UMRAO is supported in part by a series of grants from the NSF, most recently AST-0607523, and by funds from the University of Michigan Department of Astronomy.

References

Aller, M. F., Aller, H. D., & Hughes, P. A. 2003, ApJ, 586, 33
Aller, M. F., Aller, H. D., Hughes, P. A., & Latimer, G. E. 1999, ApJ, 512, 601

Ciaramella, A., Bongardo, C., Aller, H. D., et al. 2004, A&A, 419, 485
Hartman, R. C., Bertsch, D. L., Bloom, S. D., et al. 1999, ApJS, 123, 79
Hovatta, T., Tornikoski, M., Lainela, M., et al. 2007, A&A, 469, 899
Hughes, P. A., Aller, H. D., & Aller, M. F. 1985, ApJ, 298, 301
Hughes, P. A., Aller, H. D., & Aller, M. F. 1992, ApJ, 396, 469
Kembhavi, A. K., & Narlikar, J. V. 1999, Quasars and active galactic nuclei: an introduction, ed. A. K. Kembhavi, & J. V. Narlikar (Cambridge, UK: Cambridge University Press)
Lainela, M. 1994, A&A, 286, 408
Lainela, M., & Valtaoja, E. 1993, ApJ, 416, 485
Lindfors, E. J., Türler, M., Valtaoja, E., et al. 2006, A&A, 456, 895
Marscher, A. P., & Gear, W. K. 1985, ApJ, 298, 114
Mattox, J. R., Hartman, R. C., & Reimer, O. 2001, ApJS, 135, 155
Nieppola, E., Tornikoski, M., Lähteenmäki, A., et al. 2007, AJ, 133, 1947
Nieppola, E., Hovatta, T., Tornikoski, M., et al. 2008, A&A, submitted
Pyatunina, T. B., Kudryavtseva, N. A., Gabuzda, D. C., et al. 2006, MNRAS, 373, 1470
Pyatunina, T. B., Kudryavtseva, N. A., Gabuzda, D. C., et al. 2007, MNRAS, 381, 797
Reuter, H.-P., Kramer, C., Sievers, A., et al. 1997, A&AS, 122, 271
Salonen, E., Teräsranta, H., Urpo, S., et al. 1987, A&AS, 70, 409
Steppe, H., Salter, C. J., Chini, R., et al. 1988, A&AS, 71, 317
Steppe, H., Liechti, S., Mauersberger, R., et al. 1992, A&AS, 96, 441
Steppe, H., Paubert, G., Sievers, A., et al. 1993, A&AS, 102, 611
Stevens, J. A., Litchfield, S. J., Robson, E. I., et al. 1994, ApJ, 437, 91
Teräsranta, H., Tornikoski, M., Valtaoja, E., et al. 1992, A&AS, 94, 121
Teräsranta, H., Tornikoski, M., Mujunen, A., et al. 1998, A&AS, 132, 305
Teräsranta, H., Achren, J., Hanski, M., et al. 2004, A&A, 427, 769
Teräsranta, H., Wiren, S., Koivisto, P., Saarinen, V., & Hovatta, T. 2005, A&A, 440, 409
Tornikoski, M., Valtaoja, E., Terasranta, H., et al. 1993, AJ, 105, 1680
Tornikoski, M., Valtaoja, E., Teräsranta, H., et al. 1996, A&AS, 116, 157
Tornikoski, M., Lainela, M., & Valtaoja, E. 2000, AJ, 120, 2278
Türler, M., Courvoisier, T. J.-L., & Paltani, S. 1999, A&A, 349, 45
Türler, M., Courvoisier, T. J.-L., & Paltani, S. 2000, A&A, 361, 850
Valtaoja, E., Haarala, S., Lehto, H., et al. 1988, A&A, 203, 1
Valtaoja, E., Teräsranta, H., Urpo, S., et al. 1992a, A&A, 254, 71
Valtaoja, E., Teräsranta, H., Urpo, S., et al. 1992b, A&A, 254, 80
Valtaoja, E., Lähteenmäki, A., Teräsranta, H., & Lainela, M. 1999, ApJS, 120, 95